

Room temperature CO₂ gas sensors of AuNPs/mesoPSi hybrid structures

Alwan M. Alwan¹ · Amer B. Dheyab²

Received: 20 March 2017 / Accepted: 6 June 2017 / Published online: 17 July 2017
© The Author(s) 2017. This article is an open access publication

Abstract Mesoporous silicon (mesoPSi) layer prepared by a laser-assisted etching process in HF acid has been employed as CO₂ gas sensors. The surface morphology of mesoPSi was modified by embedding gold nanoparticles AuNPs by simple and quick dipping process in different gold salts concentrations to form mesoPSi/AuNPs hybrid structures. Morphology of hybrid structures was investigated using scanning electron microscopy (SEM) and X-ray diffraction (XRD). The electrical characteristics of the prepared gas sensor were carried out at room temperature. It was found that the nanoparticles size, shape and the specific surface area of the nanoparticle strongly influence the current–voltage characteristics. Considerable improvement was noticed in sensitivity, response and recovery times of gas sensor with decreasing incorporated AuNPs into the mesoPSi matrix.

Keywords MesoPSi · SEM · Laser-assisted etching · AuNPs hybrid structures · Gas sensing

Introduction

Porous silicon gas sensors for continuous monitoring of CO₂ in the air environment are of great importance as a global issue. The development of inexpensive, stable, high-sensitivity Psi-based sensor operating at the room temperature is an important problem (Gabouze et al. 2005;

He et al. 1997; Holzinger et al. 1997; Liu and Weppner 1990; Lee et al. 1995; Kale et al. 1996; Gabouzea et al. 2006). The performance of the Psi gas sensor depends upon the morphological properties of surfaces, including pore shape, diameter and uniformity of the porous surface in addition to the thickness of the porous layer (Martinez et al. 2008). The modification of Psi layer by incorporation of nano-structured metal and the metal oxides layer has been found as an efficient process to improve the gas-sensing performance (SerdarOzdemira and James 2008; Ozdemir and Gole 2010). The Psi side of the substrate is then coated with a thin layer of gold. These devices, which run at room temperature, are extra sensitive to the applied voltages in CO₂ gas, which show that the conductivity and also nano-structured Psi have greater response than the others.

Zouadi et al. have stated the role of hydrocarbon groups (CH_x) thickness layer on detection process of CH_x/Psi/Si structures in the presence of CO₂ gas (Zouadi et al. 2013). The fabrication Psi was presented with nano- and microstructures as carbon dioxide sensing layers (Naama et al. 2015). More recently, Naama et al. studied the performance of silicon nano-wires modification with gold and platinum nanoparticles as a CO₂ gas sensor, and it is shown that the sensor performance depends powerfully on the alteration of metal nanoparticle type (Naama et al. 2015).

In the current research, we report on the fabrication and characteristics study of (AlmesoPSi/AuNPs n-Si/Al) hybrid structures as CO₂ gas sensors working at room temperature. The role of incorporation of AuNPs of different sizes and morphologies in a porous matrix on enhancing the performance of the hybrid sensors has been studied and analyzed extensively.

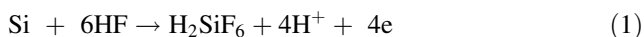
✉ Alwan M. Alwan
amer.aljoburi@yahoo.com

¹ School of Applied Science, University of Technology, Baghdad, Iraq

² Ministry of Science and Technology, Baghdad, Iraq

Fabrication and Experimental

Single-crystalline mirror-like n-type silicon wafers of a resistivity 10 Ωcm and (100) orientation were used in this work. The silicon substrates were cut into square samples of (2 cm \times 2 cm) area. Prior to the etching process, the native oxide was removed from the silicon substrate in 10% HF solution. The backside of silicon substrates was coated with 0.2- μm -thick high-purity aluminum film by a thermal deposition process. Mesoporous silicon layers were fabricated by a laser-assisted etching technique using a mixture containing 40% HF and 99.99% ethanol, 1:1, as the electrolyte. The silicon substrate and platinum cathode were kept perpendicular to each other with a distance of (0.8 cm) between them in a Teflon cell to form homogeneous mesoPSi layers. The silicon substrates were etched at a current density of 18 mA/cm² for 15 min under 630 nm laser wavelength and 20 mW/cm² illumination. After formation, the mesoPSi substrates were rinsed in distilled water and allowed to dry at ambient air. Gold nanoparticles (AuNPs/mesoPSi) were deposited on mesoPSi layer through an ion reduction process of immersing the interface into different aqueous solutions of HAuCl₄/HF acid, sample (S₁) with (1 mM/3M) and sample (S₂) with (10 mM/3M) for 5 min at room temperature. The reduction process of AuNPs by the dangling bonds of the porous layer is given by the equations (Adawiyah et al. 2016; Ismail et al. 2017):



Finally, the resulting AuNPs/mesoPSi hybrid structures were washed with deionized water and dried with N₂ ambient. The front electrical contact over the AuNPs/mesoPSi layer is carried out by deposition of a thin layer of aluminum. Figure 1 shows the schematics of AuNPs embedded in the mesoPSi layer. Morphological properties of AuNPs and mesoPSi were studied using scanning electron microscopy (SEM) image (JM-5600) fortified with an energy-dispersive X-ray analysis device. The structural characteristics were investigated by means

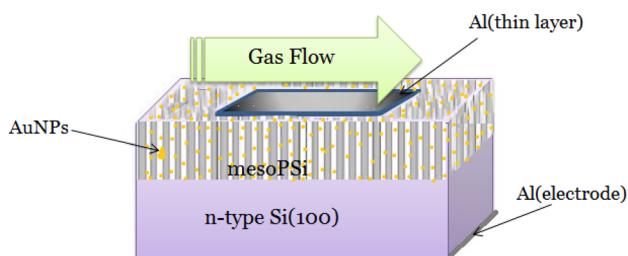


Fig. 1 Schematic representation of Al/AuNPs-mesoPSi/n-Si/Al hybrid structure

of XRD-6000, Shimadzu X-ray diffractometer. The hybrid samples were kept in a small sealed chamber with an inlet and outlet provision of gases. The pressure of CO₂ gas in the chamber was about 0.5 mbar and 1 mbar. The current–voltage characteristics were investigated under dark at room temperature by a fine DC power supply at 8846 flukes 6–1/2 digit precision multimeter. The silicon wall size and the AuNPs sizes were estimated using special software program Image J version 8.

Results and discussion

Structural characterization

The XRD pattern of AuNPs deposited on the mesoPSi layer is given in Fig. 2.

It is obviously seen that the grown-up AuNPs are polycrystalline in nature and have specific diffraction peaks at (38.45°) and (44.4°) for sample (S₁), while for sample (S₂), the peaks are (38.8°) and (44.8°) that correspond to (111) and (200) diffraction planes, respectively, belonging to the AuNPs of F.C.C structure.

The XRD pattern of AuNPs agrees with reported data (Rallos 1998). The XRD peaks of the sample (S₁) are lower than those of sample (S₂) due to the fact that the density of AuNPs and their nucleation sites increased with HAuCl₄ salt concentration.

The average (*D*) grain sizes of gold particles were calculated from the peak broadening, and it can be obtained by means of Scherrer's formula as follows (Alwan and Hayder 2015):

$$D = 0.89\lambda / (\beta \cos \theta) \quad (3)$$

where λ is the wavelength in (nm) of employed radiation, β (in radians) is the full width at half maximum (FWHM), θ (in radians) is the diffraction angle, and 0.89 is the shape factor value. The specific surface area (SSA) is one of the figures of the merit of the material and it is given as (Ben-Chorin 1994):

$$\text{SSA} = \frac{6000}{D * \rho} \quad (4)$$

where ρ is the density of gold (19.3 g/cm³).

The AuNPs sizes, full width half maximum (FWHM) and specific surface area (SSA) are presented in Table 1.

The lower AuNPs size and therefore higher SSA were attained from the sample (S₁) of lower HAuCl₄ salt concentration due to the fact that the dimmers process is decreased with a dilution of salt concentration. The surface morphology of mesoPSi layer before incorporation of AuNPs is illustrated in Fig. 3; it is clear that the porous layer seems as a circular pore-like structure with a uniform

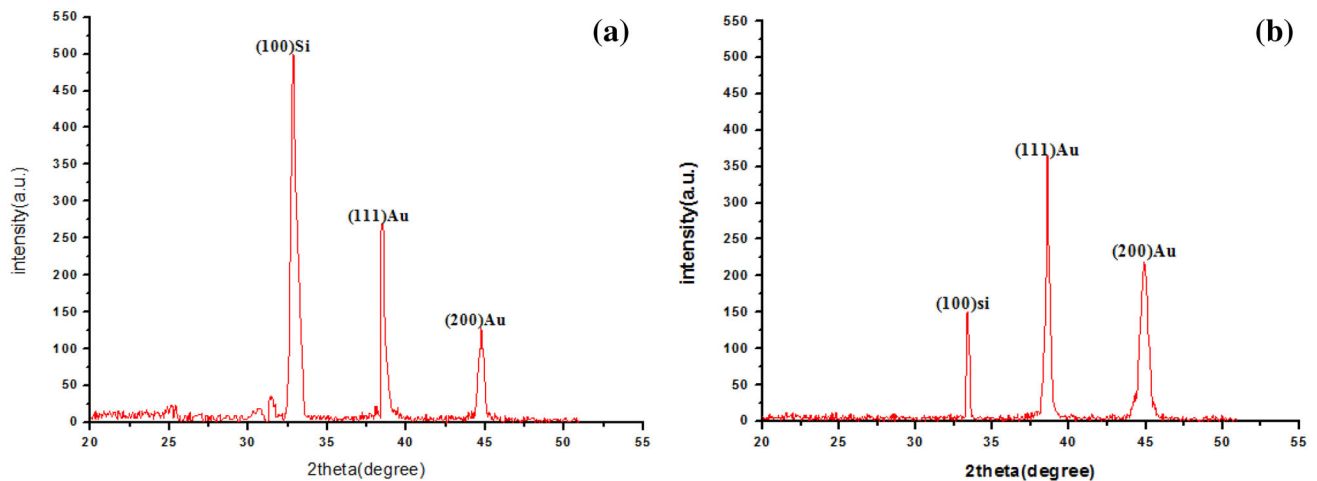


Fig. 2 XRD pattern of AuNPs formed by dipping mesoPSi in **a** sample (S_1), **b** sample (S_2)

Table 1 Grain size, FWHM and specific surface area (SSA) of AuNPs

Sample	Plane (111)			Plane (200)		
	FWHM (rad)	Size of AuNPs (nm)	SSA of AuNPs (m^2/g)	FWHM (rad)	Size of AuNPs (nm)	SSA of AuNPs (m^2/g)
S_2	0.01	14	23.5	0.018	8.1	38.1
S_1	0.038	5	66.1	0.023	6.7	46.7

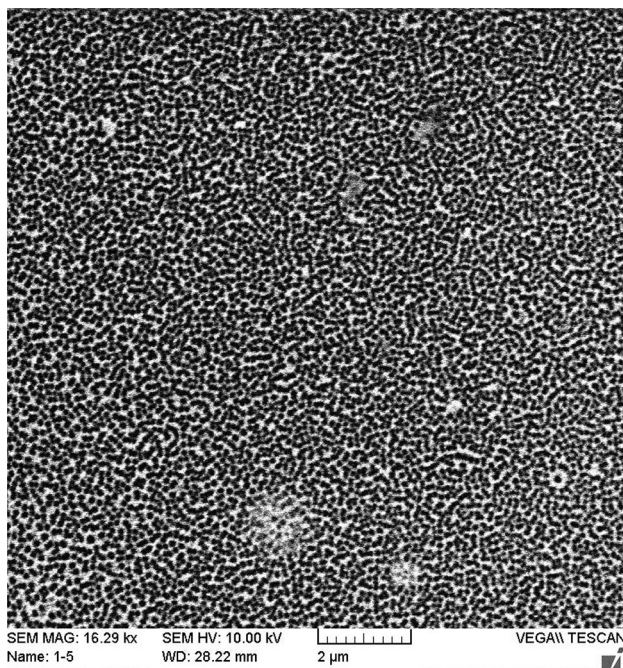


Fig. 3 SEM images of as-formed mesoPSi. *Inset* is the statistical distribution of pores sizes

distribution over the surface. The statistical distribution of the pore sizes ranges from 0.025 to 0.675 μm , and the peak of the distribution is about 0.125 μm . The porosity was calculated by gravimetric method (Ben-Chorin 1994) and

was about 74%; the silicon wall size was estimated to be about 50 nm.

Figure 4a, b shows the SEM images of AuNPs on the mesoPSi layer. It is clear that the created AuNPs have different morphologies of various particles sizes and shape. As shown in Fig. 4, the particles are vastly uniformly distributed outside the walls of silicon inside the porous matrix. In Fig. 4b for sample S_1 at the distribution was varied from 0.1 to 1.5 μm and the peak of the distribution located at 0.1 μm , while for figure 4b for sample S_2 at the distribution was varied from 0.05 to 1.25 μm and the peak of the distribution located at 0.05 μm , it can be definitely distinguished that the particles are highly agglomerated over the porous silicon surface, so the porous are fully covered by AuNPs. The average particle size was around 1 μm .

From cross-sectional SEM images, AuNPs are demonstrated in Fig. 5a, b. From this figure, it is easy to distinguish that the AuNPs are positioned inside the individual pores, and the AuNPs progress follows the aqueous solutions of $H AuCl_4/HF$ acid.

Figure 5a shows that AuNPs decorate the inside of the pores walls. Moreover, Fig. 5b views that the separated gold nano-aggregates are formed (islands of AuNPs). This can be due to the increase in the gold ions reduction process.

The EDX spectra of AuNPs deposited on mesoPSi are presented in Fig. 6a, b, this figure confirms the growth of AuNPs and the presence of Si and O elements, and no other elements were found. The intensity of AuNPs peak in

Fig. 4 SEM images of AuNPs. *Inset* is magnified SEM images of AuNPs. **a** Sample S₁, **b** sample S₂

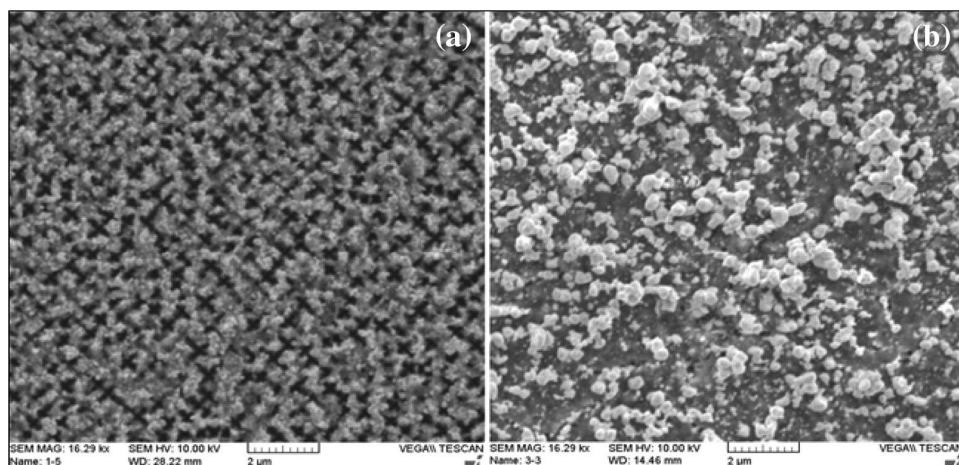


Fig. 5 Cross-sectional SEM images of AuNPs deposited on mesoPSi. **a** Sample S₁, **b** sample S₂

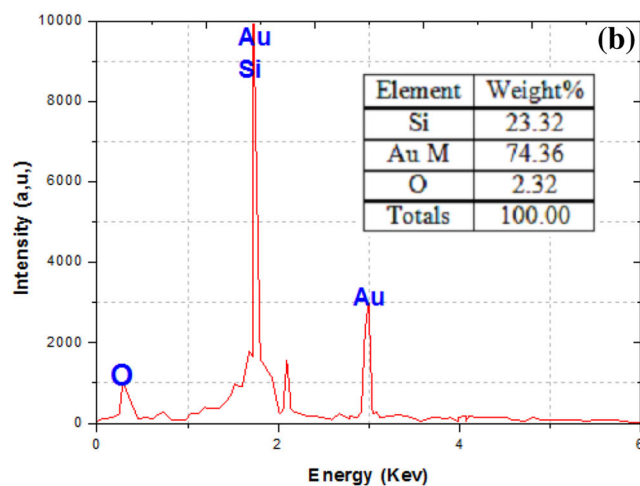
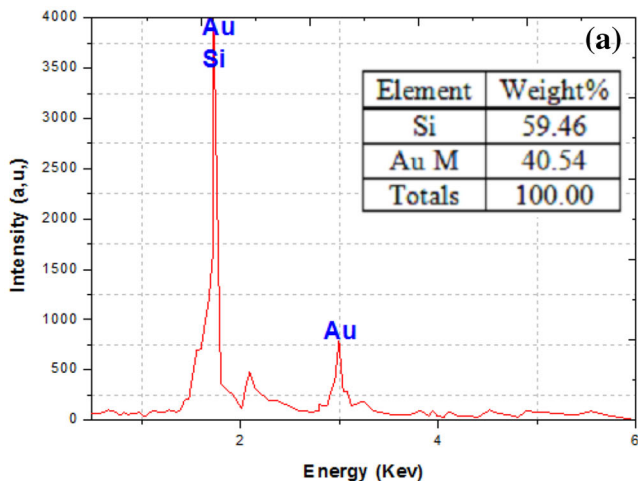
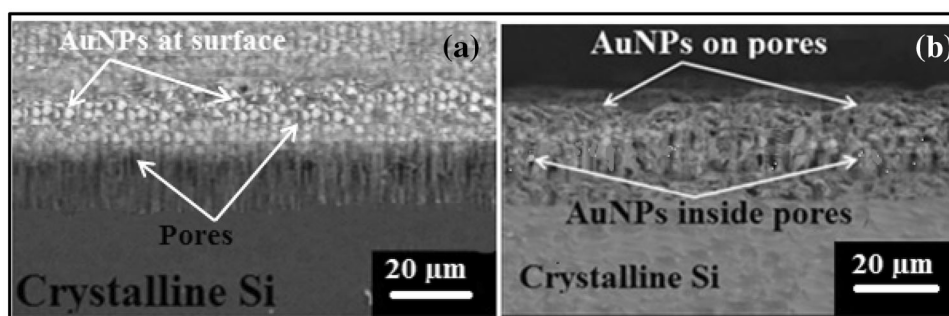


Fig. 6 EDX spectra of AuNPs embedded in the porous matrix. **a** Sample S₁, **b** sample S₂

sample S₂ is higher than that of sample S₁, indicating that the AuNPs in sample S₁ deposited at a low rate compared to sample S₂.

Electrical characterization

The effects of incorporation of AuNPs on the porous matrix on the current–voltage (I–V) characterization of Al/AuNPs/

mesoPSi/Al at room temperatures are demonstrated in Fig. 7b, c, while Fig. 7a illustrates the characterization of a mesoPSi layer of Al/mesoPSi/Al structure before embedding of AuNPs. It can be noted for as-formed mesoPSi, the I–V characteristic exhibits an ohmic contact behavior.

The deposition of resulted AuNPs improved the rectification properties with increasing the forward current with applied voltage due to the presence of Schottky structure

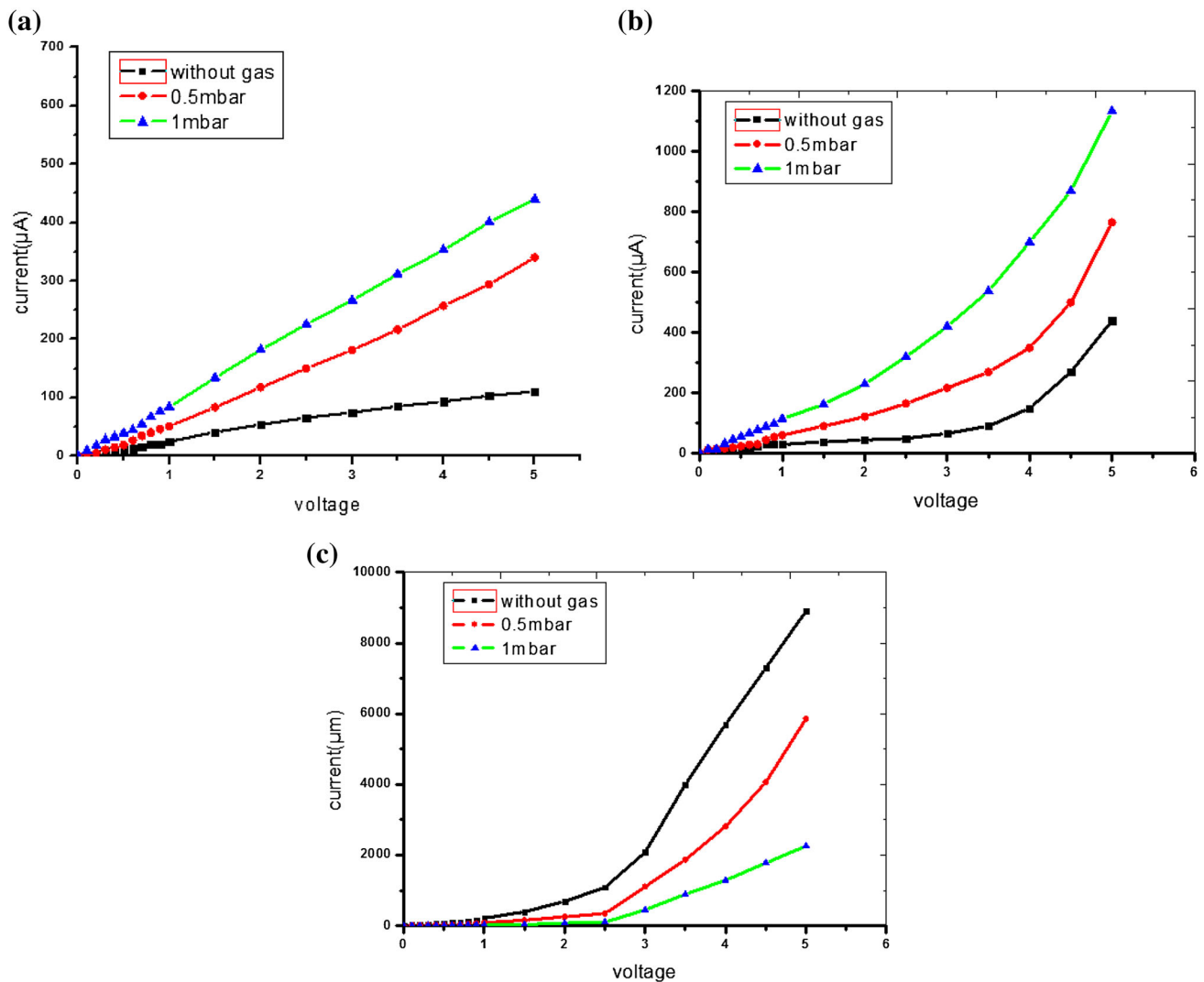


Fig. 7 Forward current–voltage characteristics of **a** as-formed mesoPSi and AuNPs modified structures, **b** sample S₁, **c** sample S₂

and decreasing the resistivity of the porous layer (Sadr et al. 2013).

As shown in Fig. 7, the adsorption of the CO₂ gas molecule has a significant effect on the I–V characteristics of Al/mesoPSi/n-Si/Al and Al/AuNPs/mesoPSi/n-Si/Al structures. The incorporation of AuNPs of sample S₁ causes increase in forwarding current with increasing CO₂ gas concentration in the chamber compared with sample S₂ in which the adsorption of gas molecules leads to decrease in the forward current. There are several approaches to explain the increasing current in the presence of CO₂ gas. For activation of the charge carriers trapping due to adsorbate interaction with porous silicon dangling bond, Si–H states lead to enhancement of the conductance variations due to the trapping or release of the carriers (Sadr et al. 2013). This variation is connected to the desorption of

the CO₂ molecule on the porous silicon layer owing to the van der Waals interaction. The CO₂ desorption will lead to change in the dielectric constant of the porous layer. The dependence of the dielectric $\epsilon_{r\text{PSi}}$ on the porosity of the porous layer and the embedding medium ($\epsilon_{r\text{pore}}$) is given by Eq. (5) (Canham 1997).

$$\epsilon_{r\text{PSi}} = (1 - P\%) \epsilon_{r\text{Si}}^{1/3} + P\% \epsilon_{r\text{pore}}^{1/3} \quad (5)$$

where P % is the porosity of the porous layer and the $\epsilon_{r\text{pore}}$ is the dielectric constant of the embedding medium (CO₂ molecule). Furthermore, the AuNPs deposited on the walls of the silicon in the porous matrix act as an additional source to improve the surface area and hence enhance the gas adsorption rate (Zhang and Chu 2014), while the embedded gold nanoparticle inside the pores itself will damp the activity of the pores, so the current will decrease.

The relative response of the current of the (S) was calculated using the following relation:

$$S = \left| \frac{I_g - I_v}{I_v} \right| \quad (6)$$

where I_g and I_v represent the current in the presence and absence of CO_2 gas, respectively. The response–voltage characteristics of the samples permit defining the applied voltage range corresponding to the optimum response. Figure 8a–c shows the response–voltage characteristics of Al/mesoPSi/n-Si/Al and Al/AuNPs/mesoPSi/n-Si/Al structures under two concentrations of CO_2 gas at room temperature. As shown in Fig. 8a–c, the relative response of the structures grows with concentrations of gas molecules. The maximum response was obtained for a sensor of smallest AuNPs sample (S_1) compared with the other sensors fully covered by largest AuNPs sample S_2 . The high sensitivity is observed at a bias voltage of about 2.5 V for sample S_1 compared to 5 and 0.35 V for as-formed

mesoPSi sample and mesoPSi embedding with largest sizes of AuNPs sample S_2 , respectively. This can be ascribed to the presence of Schottky structure; the forward current is intensively controlled by the change in barrier height, which formed between the AuNPs layer of sample S_2 and the mesoPSi at low bias voltage and organized by specific surface area of both of AuNPs and a mesoPSi layer of sample S_1 .

The temporal response characteristics of the samples were measured for two concentrations at room temperature; Fig. 9 displays the transient response of Al/mesoPSi/n-Si/Al and Al/AuNPs/mesoPSi/n-Si/Al structures under two concentrations of CO_2 (0.5 and 1 mbar) at the own best biasing voltage. This figure also illustrates that the response increases with the concentration of the gas for all samples. Table 2 demonstrates the values of the temporal response for all samples. It can be distinguished that they are lower for AuNPs modified structures sample S_1 compared with the other samples. The considerable short time of response

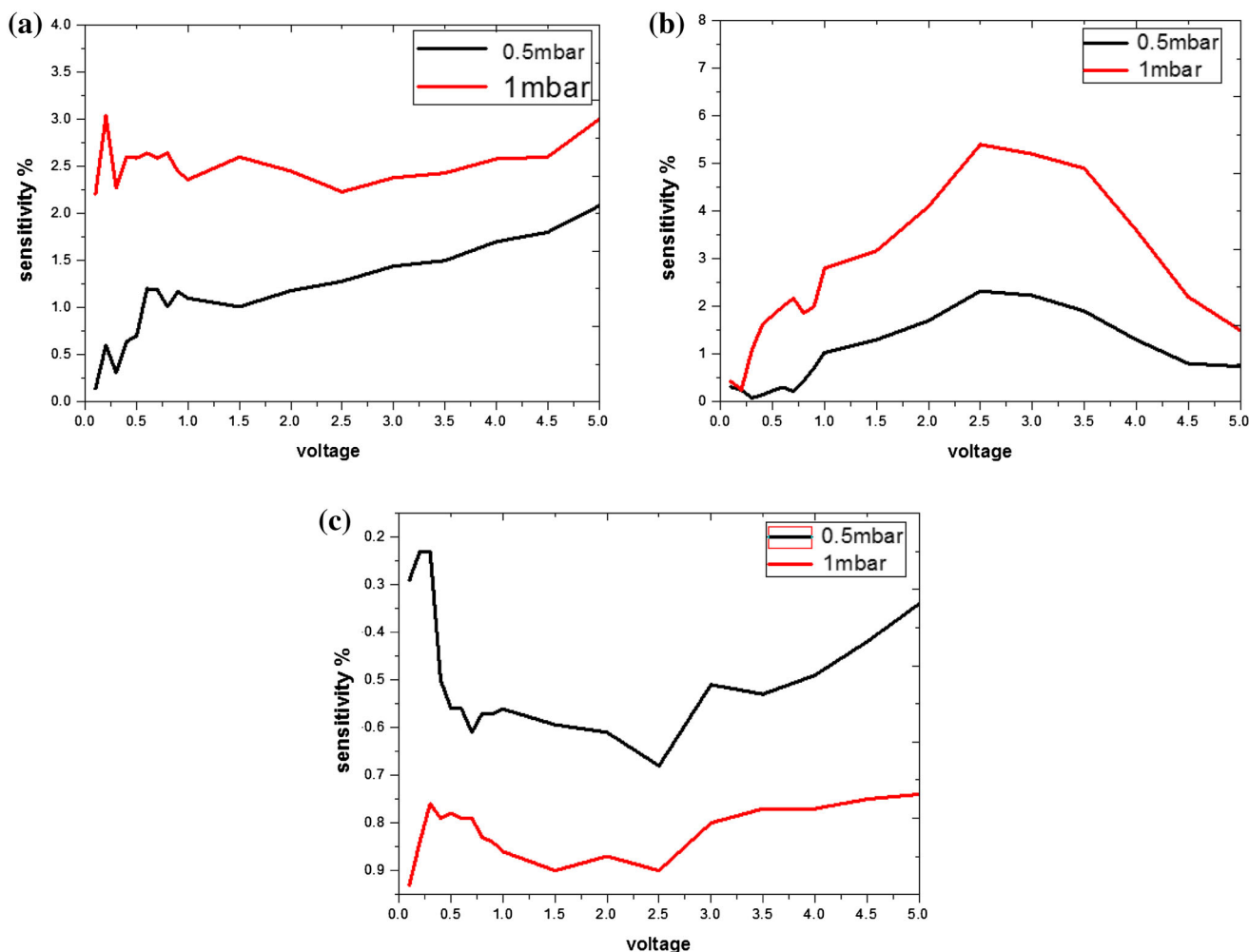


Fig. 8 Response–voltage characteristics of **a** as-formed mesoPSi and AuNPs modified structures, **b** sample S_1 , **c** sample S_2

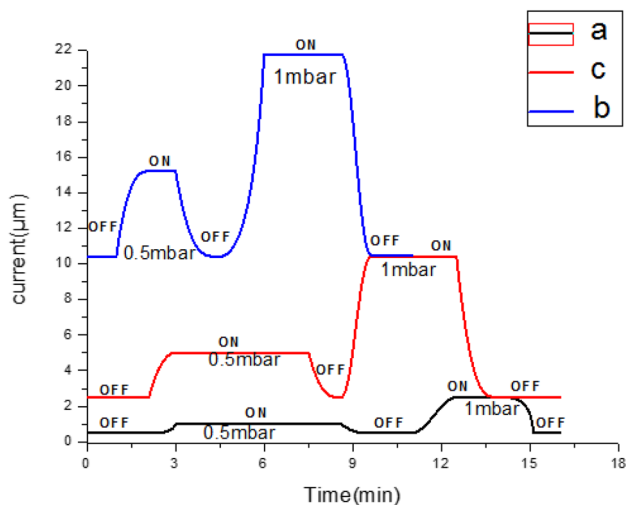


Fig. 9 Temporal response characteristics at two concentrations 0.5 and 1 mbar of **a** as-formed mesoPSi and AuNPs modified structures, **b** sample S₁, **c** sample S₂

Table 2 Temporal response of as-formed mesoPSi and AuNPs modified structures sample S₁ and sample S₂

Sample	Concentration CO ₂			
	Temporal response (min)		Recovery time (min)	
	0.5 mbar	1 mbar	0.5 mbar	1 mbar
As-formed mesoPSi	0.4	0.59	0.61	0.64
AuNPs modified sample S ₁	0.3	0.72	0.5	0.51
AuNPs modified sample S ₂	0.5	1.1	0.8	0.8

and recovery of sample S₁ may be due to the high rate of CO₂ gas adsorption and desorption, respectively.

Conclusion

In this work, mesoPSi/AuNPs-psi hybrid CO₂ gas sensor structures were fabricated in sandwich structure configuration Al/AuNPs/mesoPSi/n-Si/Al. Surface modification process, after mesoPSi which was prepared by a laser-assisted etching process, was carried out by incorporating different sizes and morphologies of AuNPs. The simple immersion process of mesoPSi in different HAuCl₄/HF solution concentrations was employed to synthesize AuNPs. It has been observed that the sensor response depends powerfully on the morphology and the Au nanoparticle sizes. Maximum sensitivity with the minimum response and recovery times was obtained with smallest Au nanoparticle sizes deposited at the walls of silicon rather than inside the pores itself.

Open Access This article is distributed under the terms of the Creative Commons Attribution 4.0 International License (<http://creativecommons.org/licenses/by/4.0/>), which permits unrestricted use, distribution, and reproduction in any medium, provided you give appropriate credit to the original author(s) and the source, provide a link to the Creative Commons license, and indicate if changes were made.

References

- Adawyia JH, Alwan MA, Allaa AJ (2016) Optimizing of porous silicon morphology for synthesis of silver Nanoparticles. *Microporous Mesoporous Mater* 227:152–160
- Alwan AM, Hayder AJ, Jabbar AA (2015) Study on morphological and structural properties of silver plating on laser etched silicon. *Surf Coat Technol* 283:22–28
- Ben-Chorin M, Moller F, Koch F (1994) *Phys Rev B* 49:2981
- Canham LT (1997) *Properties of porous silicon*. Published by: INSPEC, The Institution of Electrical Engineers, London, United Kingdom 1997
- Gabouze N, Belhousse S, Cheraga H (2005) *Phys State Solidi (C)* N9:3449
- Gabouze N, Belhousse S, Cheraga H, Ghellaib N, Ouadaha Y, Belkacema Y, Keffousa A (2006) CO₂ and H₂ detection with a CHx/porous silicon-based sensor. *Vacuum* 80:986–989
- He G, Narushima T, Iguchi Y, Goto T, Hirai T (1997) 11th International conference on solid state ionics, Waikiki Beach, Honolulu, Hawaii
- Holzinger M, Maier J, Sitte W (1997) *Solid State Ionics* 74:217
- Ismail Raid A, Alwan Alwan M, Ahmed Ahmed S (2017) Preparation and characteristics study of nano-porous silicon UV Photodetector. *Appl Nanosci* 7:9–15
- Kale GM, Davidson AJ, Fray DJ (1996) *Solid State Ionics* 86–88:1107
- Lee D-D, Chooi S-D, Lee K-W (1995) *Sens Actuators B* 25–26:60
- Liu J, Weppner W (1990) *Solid State Commun* 76(3):311
- Martinez HM, Rincon NE, Torres J, Alfonso JE (2008) Porous silicon thin film as CO sensor. *Microelectron J* 39:1354–1355
- Naama S, Hadjersi T, Keffous A, Nezzal G (2015) CO₂ gas sensor based on silicon nanowires modified with metal nanoparticles. *Mater Sci Semiconduct Process* 1369–8001
- Ozdemir S, Gole JL (2010) Gas transport and response in porous silicon sensors. *Mater Res Soc Symp Proc*, vol 1253[®] Materials Research Society, 2010
- Ozdemira S, Gole JL (2008) Porous silicon gas sensors for room temperature detection of ammonia and phosphine. *ECS Trans* 16(11):379–385
- Sadr S, Azim-Araghi ME, Rahimi M, Dariani RS (2013) Effect of gold electrode annealing on gas sensing properties of nano-and microstructures of macroporous silicon. *Indian J Pure Appl Phys* 51:860–863
- Zanoni R, Righini G, Mattogno G, Schirone L, Sotgiu G, Rallos F (1998) *JOL* 80:159–162
- Zhang Y, Chu W, Foroushani AD, Wang H et al (2014) new gold nanostructures for sensor applications: a review. *Materials* 7:5169–5201
- Zouadi N, Belhousse S, Bradai D, Cheraga H, Ouchabane M, Keffous A, Sam S, Gabouze N (2013) Superlattices *Microstruct* 63:131–140